Are molecule-covered dust grains efficient catalysts of H2 formation in the cold ISM?

L. Gavilan, J. Lemaire, G. Vidali

Monthly Notices
of the
ROYAL ASTRONOMICAL SOCIETY

Mon. Not. R. Astron. Soc. **424,** 2961–2970 (2012) doi:10.1111/j.1365-2966.2012.21463.x

Are molecule-covered dust grains efficient catalysts of H_2 formation in the cold ISM?

L. Gavilan,⋆ J. L. Lemaire and G. Vidali†

LERMA/LAMAp, UMR 8112 du CNRS, de l'Observatoire de Paris et de l'Université de Cergy Pontoise 5 mail Gay Lussac, 95000 Cergy Pontoise, France

Accepted 2012 June 1. Received 2012 April 30; in original form 2012 April 7

ABSTRACT

The formation of H_2 in the interstellar medium (ISM) involves complex processes, some of which are still not understood. In cold regions, it is assumed that H_2 formation follows Langmuir kinetics, i.e. the immediate desorption of incoming atoms or molecules on a surface already saturated with molecules. Our experiments address this issue by studying the formation of H_2 on a dust surface dosed with molecules prior to atomic exposure. We simulate ISM conditions at $T_{\rm dust} < 10$ K and $T_{\rm gas} \sim 90$ K and use a synthesized amorphous silicate. By coupling laser detection to thermal desorption spectroscopy, we confirm that hydrogen recombination is promptly enhanced. We interpret this as a result of enhanced atomic diffusion (both hopping thermal and quantum mechanical tunnelling). Moreover, since H_2 formation is the most exothermic chemical reaction per unit mass, we elucidate its importance as a non-thermal desorption mechanism. We apply these results to dense ISM regions where H_2 formation and its induced desorption are curbed by a declining atomic gas-phase abundance. We further propose this as a pathway to deuterium fractionation in pre-stellar cores. More importantly, we show that dust remains an active catalyst even in the coldest ISM.

Key words: astrochemistry – molecular processes – methods: laboratory – ISM: atoms – ISM: molecules.

1 INTRODUCTION

H_2 is the most abundant molecule in the Universe and a significant fraction of its baryonic mass. H_2 formation initiates the chemistry of interstellar clouds, controlling their ionization and thermal balance, eventually enabling star formation (Dalgarno 1999). The production rate of H_2 is crucial in the early Universe where cooling through H_2 lines can provide the conditions allowing the formation of the first stars. Experimental work enriched models have constrained H_2 production in the gas phase during this epoch (Kreckel et al. 2010).

At a redshift of $z \sim 1.5$, Norman & Spaans (1997) estimated that H_2 formation in the gas phase and H_2 formation on grain surfaces become equally important. For $z \leq 1$, grain surface reactions are enhanced compared to the associative detachment of hydrogen ($H + H^- \rightarrow H_2 + e^-$) at higher redshifts (Cazaux & Spaans 2004). The recombination of H_2 on a dust grain surface (g) happens in the following steps:

$$H + g : H \rightarrow H : g : H \rightsquigarrow H - H : g \rightarrow H_2^* + g. \quad (1)$$

The first step is the sticking or thermalization of an atom on the grain surface, ':H'. This is followed by diffusion on the grain allowing atoms to encounter each other and bond. The newly formed molecule leaves the grain internally excited. In the first step, a hydrogen atom can bind to a grain surface via physisorption or chemisorption, depending on its incoming kinetic energy. In our case we examine physisorption which occurs when the attractive forces are due to mutually induced dipole moments in the electron shells of H and surface atoms (a van der Waals type interaction). In chemisorption, a covalent bond is formed when the atom and the surface wavefunctions overlap. At $T_{\rm dust} \geq 1000$ K hydrogen atoms recombine thanks to chemisorption as the high $T_{\rm gas}$ provides sufficient energy for atoms to populate chemisorbed sites. None the less, recent theoretical work (Goumans & Bromley 2011) seems to indicate that chemisorption on a silicate could be barrierless even at low $T_{\rm gas}$.

Gould & Salpeter (1963) pioneered a study on hydrogen physisorption on grains which showed that the recombination of physisorbed atoms on an ice surface is efficient between $T_{\rm dust} = 10$ and 20 K. Since there is observational evidence that molecular hydrogen

⋆E-mail: lisseth.gavilan@obspm.fr.
†Present address: Physics Department, Syracuse University, Syracuse, NY 13244, USA.

is pervasive at wider temperature ranges, hydrogen formation had to involve H atoms bound to dislocations and impurities (Hollenbach & Salpeter 1971), which also included non-thermal diffusion by tunnelling, increasing the recombination efficiency to $T_{\rm dust} = 50$ K. Modelling work (Cazaux & Tielens 2004) stressed that the mobility of atoms can be governed by a combination of quantum mechanical tunnelling and thermal hopping. The latter causes recombination to persist up to $T_{\rm dust} = 500$ K. Such theoretical studies have been done on pristine dust surfaces, such as graphite. Langmuir (1918) argued that incoming atoms, arriving on top of atoms or molecules already bound to the surface, do not bind and are ejected. This may suggest a decline in formation efficiency on colder dust, as its surface is saturated with molecules implying an immediate ejection of incoming atoms. Our experimental study addresses this long-unresolved question.

The first experimental studies on hydrogen formation on astrophysical analogues were done on icy surfaces (Lee 1972; Govers, Mattera & Scoles 1980) and more recently using H and D atoms on amorphous ice at $T = 8$ K (Hornekær et al. 2003; Roser et al. 2003). Bare surfaces have also been used to study the formation of H_2 isotopologues, initially using HD on crystalline silicates (Pirronello et al. 1997b,a) and then on amorphous carbonaceous surfaces between 5 and 20 K (Katz et al. 1999; Pirronello et al. 1999) and amorphous silicates (Perets et al. 2005; Vidali et al. 2007). All these have employed temperature programmed desorption (TPD). Laser-induced resonance-enhanced multiphoton ionization (REMPI) techniques have been used to detect excited H_2 and HD on a highly oriented pyrolytic graphite (HOPG) surface between $T_{\rm dust} = 15$ and 50 K (Perry & Price 2003; Creighan, Perry & Price 2006; Islam, Latimer & Price 2007; Latimer, Islam & Price 2008). These studies mapped the nascent rovibrational distribution of HD up to $v'' = 7$, $J'' = 7$. The internal excitation of a newly formed H_2 molecule is used in its detection via REMPI, effectively discerning nascent H_2 from other sources. More recently, REMPI has also been used to study D_2 on an amorphous silicate at $5.5 < T_{\rm dust} < 70$ K (Lemaire et al. 2010), showing the involvement of competing formation mechanisms.

The partition of the released energy in the formation of molecular hydrogen (4.48 eV) has important consequences in the overall thermal balance of a cloud in the interstellar medium (ISM), as the gained internal energy of the molecule is reradiated in the infrared (IR). Duley & Williams (1993) first suggested that the exoergicity of this reaction could impart energy to the grain surface, inducing evaporation. A study by Garrod, Wakelam & Herbst (2007) focused on the non-thermal desorption of product species from dust grains due to exothermic surface reactions. This model proposed that non-thermal desorption could prevent the complete freeze-out of gas species in dark clouds and make up for the gas-phase abundances of molecules (e.g. methanol) unaccounted by thermal desorption alone. Other typical non-thermal desorption mechanisms included in chemical models are cosmic-ray-induced desorption (Hasegawa & Herbst 1993) and direct photodesorption (Willacy & Millar 1998). As for experiments, examples of non-thermal desorption studies include the photodesorption of CO ices (Öberg et al. 2007) and the low-energy electron irradiation on H_2O ice films (Brown et al. 1982).

In these experiments, we study the physisorption and recombination of deuterium atoms by simulating ISM conditions such as $T_{\rm dust} = 5.5$ and 10 K and $T_{\rm gas} = 90$ K. Our aim is to quantify the effect of D_2 recombination enhancement and non-thermal desorption due to recombination on an amorphous silicate surface previously covered with fixed doses of D_2 molecules.

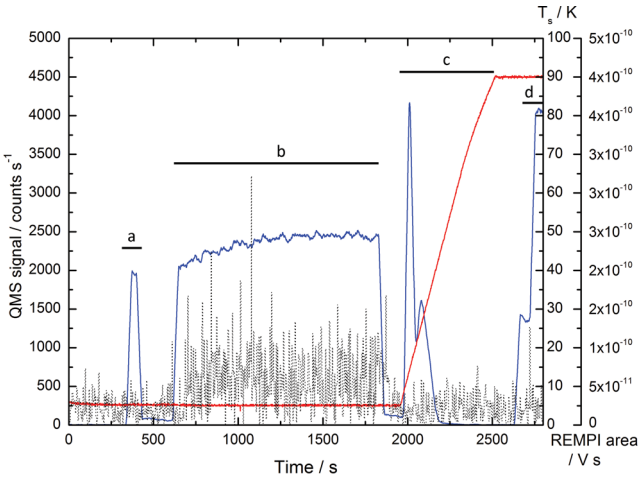

Figure 1. Scheme of one model experiment. The QMS signal is shown in blue, REMPI in black and the temperature of the surface in red. Interval (a) corresponds to the D_2 irradiation dose, (b) to the D atomic irradiation dose, (c) to the TPD and (d) to the measurement of the beam dissociation rate. The REMPI signal is the shot-by-shot laser pulse integrated area, and the noise is removed by a Haar wavelet algorithm.

2 EXPERIMENTS

For these experiments, we employ the ultra-high vacuum (UHV) Formation of Molecules in the ISM (FORMOLISM) set-up. This apparatus consists of an UHV stainless steel chamber ($<10^{-10}$ mbar). At its centre, a sample holder is thermally connected to the cold finger extension of a closed-cycle He cryostat. The sample temperature can be varied in the 5.5–350 K range and can be controlled to ± 0.2 K with an accuracy of ± 1 K.

The sample consists of an amorphous olivine-type silicate film whose chemical formula is $(Fe_x, Mg_{1-wx})_2\ SiO_4$, where $0 < x < 1$. It was provided by Dr D'Hendecourt (Institute d'Astrophysique Spatiale, Orsay) and prepared by electron beam evaporation of San Carlos olivine (Djouadi et al. 2005) on to a gold-coated substrate. Its exact chemical composition is unknown, but its amorphous structure, verified by IR spectroscopy, is characterized by a broad absorption feature around 950 $\rm cm^{-1}$. Its thickness is estimated to be 100 nm, fully covering the gold surface.

A quadrupole mass spectrometer (QMS) is used for the detection of the products entering the main chamber and desorbing from the sample. During a TPD, two peaks are visible, as seen on interval (c) of Fig. 1. The first peak corresponds to the desorption from the sample surface and the second peak corresponds to the desorption from the sample support. The second peak is removed by extrapolating the trailing edge of the surface desorption peak obtained at minimum irradiation. At this irradiation, the contribution from the holder desorption is minimal, and the first peak is unaffected.

The atomic jet is prepared in a microwave cavity and is collimated through a triply differentially pumped line. The beam is connected by a bent teflon tube to a thick aluminum cone-shaped nozzle attached to a closed-cycle He cryostat. In this way, we ensure that no light or excited molecules created in the plasma reach the surface. We checked that no excited molecules are detected in the beam, either at room temperature or at 50 K. The experimentally estimated D_2 beam flux is 9×10^{12} molecules $\rm cm^{-2}\ s^{-1}$, measured with a pressure gauge as the residual pressure of the jet enters the main chamber. The D_2 dissociation rate of the microwave discharge is checked regularly during the experiments (typically 70 per cent),

measured by the QMS crossing the beam as the discharge is turned on and off. During the irradiation phase, the sample is exposed to a flux of 1.35×10^{13} D-atoms cm^{-2} s^{-1} (Amiaud et al. 2007; Accolla et al. 2011). For REMPI measurements, the QMS is moved above the sample to avoid perturbing the electric field in the time-of-flight (TOF) spectrometer. The background pressure during both deposition and TPD experiments is measured in this remote position. TPDs are performed using a 10 K min^{-1} linear heating ramp, and the D_2, HD and H_2 signals are recorded.

To measure the rovibrational excitation of the molecules leaving the surface, we used REMPI coupled with TOF mass spectroscopy. An ultraviolet (UV) laser beam is tuned to ionize and selectively detect a given rovibrational state via two-photon absorption through a virtual state followed by ionization: (2+1) REMPI. In this way, we sample the population of D_2 formed in the $v'' = 4$, $J'' = 2$ rovibrationally excited state of the ground state. This transition has been chosen for its suitable Franck– Condon factor (Fantz & Wunderlich 2004). A tunable dye laser pumped with the second harmonic of an Nd:YAG laser (2 J/20 Hz) followed by frequency mixing gives 222.6 nm photons with 200–300 μJ pulse^{-1}. The laser beam is focused 4 mm away from the centre of the surface. At the exit of the main chamber, the shot-by-shot laser pulse integrated power appears rather stable (7 per cent) over a few hours. The REMPI-TOF signal is recorded and integrated using a digital oscilloscope.

An ancillary set-up is composed of a hot molecular hydrogen lamp and a TOF spectrometer with characteristics very similar to the one in the main apparatus (Malmasson 1994). The source provides rovibrationally excited states (Schermann et al. 1994) by dissociating hydrogen on a 2900-K tungsten filament followed by recombination and thermalization on the cooled walls. The laser light is diverted to this set-up for wavelength adjustment and REMPI signal intensity calibration. The gas flux and the UV laser power are permanently recorded.

We devised a series of experiments aimed to understand the effect of D_2 pre-coverage on D_2 recombination. We begin each experiment by irradiating the silicate surface with a dose of D_2 molecules as soon as the surface is cooled down to 5.5 or 10 K. These doses consist of letting the D_2 gas irradiate the surface for a total time ranging from 30 to 600 s at $T_{\rm dust} = 5.5$ K, from 30 to 300 s at $T_{\rm dust} = 10$ K and a single irradiation of 120 s at $T_{\rm dust} = 16$ K, where the maximum irradiation time is limited by a faster surface saturation. The main valve, controlling the admission of D_2 into the main chamber from the jet, is closed and after a short evaporation wait (letting the QMS signal return to zero) we begin irradiation with D atoms, followed by a TPD to 90 K. Additional TPDs were done separately to calibrate each dose of D_2 molecules on the bare silicate and to characterize the new binding sites available for D_2 recombination.

The analysis of the QMS signal (all D_2 molecules in the gas phase in the chamber, in all quantum states) and the REMPI-TOF signal (only nascent, excited D_2 molecules) was done at specific intervals, shown in Fig. 1. The REMPI signal has an approximate quadratic dependence on the number of photons (laser power) and a linear dependence on the flux of D atoms. The original signal was carefully normalized by fluctuations on both parameters, given by equation (1), which shows that the REMPI (2+1) process has an ion yield approximately given by (Demtröder 1991; Pozgainer, Windholz & Winkler 1994)

$$N_{\rm i} = C N_0 \sigma_{\rm 2ph} I_{\rm ex}^2 \frac{\sigma_{\rm ion} I_{\rm ion}}{\sigma_{\rm ion} I_{\rm ion} + A}, \quad (2)$$

where N_0 is the ground state number density and C is the instrumental ion detection efficiency. $\sigma_{\rm 2ph}$ and $\sigma_{\rm ion}$ are the cross-sections for the two-photon excitation process and the ionization process, respectively. $I_{\rm ex}$ and $I_{\rm ion}$ are the photon flux densities for excitation (221 nm) radiation and ionization (which in our case is also 221 nm). A is the spontaneous fluorescence decay rate from the excited state. Typical cross-sections for two-photon processes are 10^{-30} to 10^{-36} cm^4 W^{-1}. The laser beam is pulsed every 50 ms for 10 ns, and we record the integrated signal of each pulse. This is the main drawback of the REMPI-TOF detector since it only probes about one in every five million newly formed molecules. We corrected the REMPI-TOF data using a power law to account for its non-linear dependence with laser power. We strongly smoothed the signal to visualize its positive fluctuations over the noise. Another source of noise is due to the random desorption of excited molecules. Consequently, the REMPI signal has a larger error bar (∼10 per cent) than the QMS signal (∼2 per cent).

3 RESULTS

3.1 Irradiation with deuterium molecules

The surface coverage with D_2 molecules is limited by the saturation fluence, the maximum number of particles that can be stuck on the surface at a given temperature. The QMS signal has a sharp rise when the surface reaches steady-state coverage (see Fig. 2). At this point, D_2 molecules will elastically collide with the surface because of the very low binding energies, returning immediately to the gas phase. This happens at a fluence of 2×10^{15} molecules cm^{-2} (after 250 s) at $T_{\rm dust} = 5.5$ K and a fluence of 5×10^{14} molecules cm^{-2} (after 70 s) at $T_{\rm dust} = 10$ K. Although we are exposing with a few monolayers (a maximum of five exposed monolayer (ML) at 5.5 K and 2.5 exposed ML at 10 K) only a fraction of the silicate is covered with molecules due to the lowered sticking coefficient of D_2 molecules on the surface. The actually stuck doses correspond to a sub-monolayer coverage according to their integrated TPD profiles.

We characterize the surface coverage of each dose by means of a TPD experiment (Fig. 3, left-hand panel), which characterizes the distribution of adsorption energies of molecules on the surface. The thermal desorption profile can be described by the Polanyi–Wigner equation of the desorption rate, r,

$$r = -\frac{{\rm d}N}{{\rm d}t} = A N^n {\rm e}^{(-E_{\rm ads}/k_{\rm B}T)}, \quad (3)$$

which defines the adsorption energy $E_{\rm ads}$, also known as the activation barrier for desorption. A is the pre-exponential factor describing the desorption efficiency, N is the number of adsorbed molecules on the surface, n is the order of the desorption kinetics, $k_{\rm B}$ is the Boltzmann constant and T is the temperature of the surface.

The maximum desorption signal will be given when

$$-\frac{{\rm d}N}{{\rm d}T} = \frac{A N^n}{\beta} {\rm e}^{(-E_{\rm ads}/k_{\rm B}T)} \quad (4)$$

is set to 0. Here β denotes the temperature heating ramp of 0.16 K s^{-1}. In the case of molecular adsorption, we assume first-order desorption kinetics or $n = 1$, and rearrange equation (4) to obtain

$$\frac{E_a}{k_{\rm B} T_0^2} = \frac{A}{\beta} {\rm e}^{(-E_{\rm ads}/k_{\rm B}T_0)}, \quad (5)$$

where T_0 is the temperature at which the desorption maximum occurs. At this peak, the temperature is independent of the initial coverage.

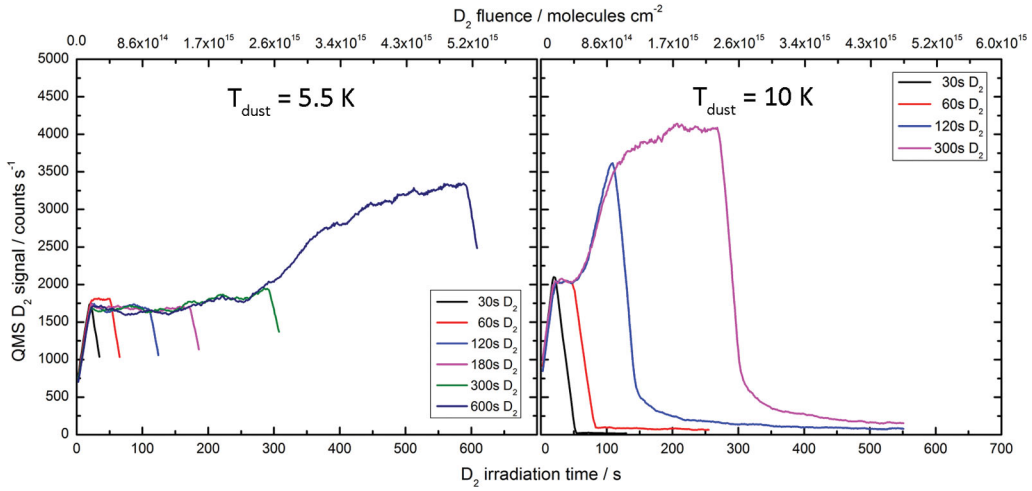

Figure 2. QMS signal (mass 4 a.m.u.) during D_2 irradiation of the silicate sample at $T_{\rm dust} = 5.5$ K (left) has a discontinuity after 250 s irradiation and after 70 s at $T_{\rm dust} = 10$ K (right). These discontinuities show the surface saturation. The drop-off signals on the right-hand side show the termination of irradiation.

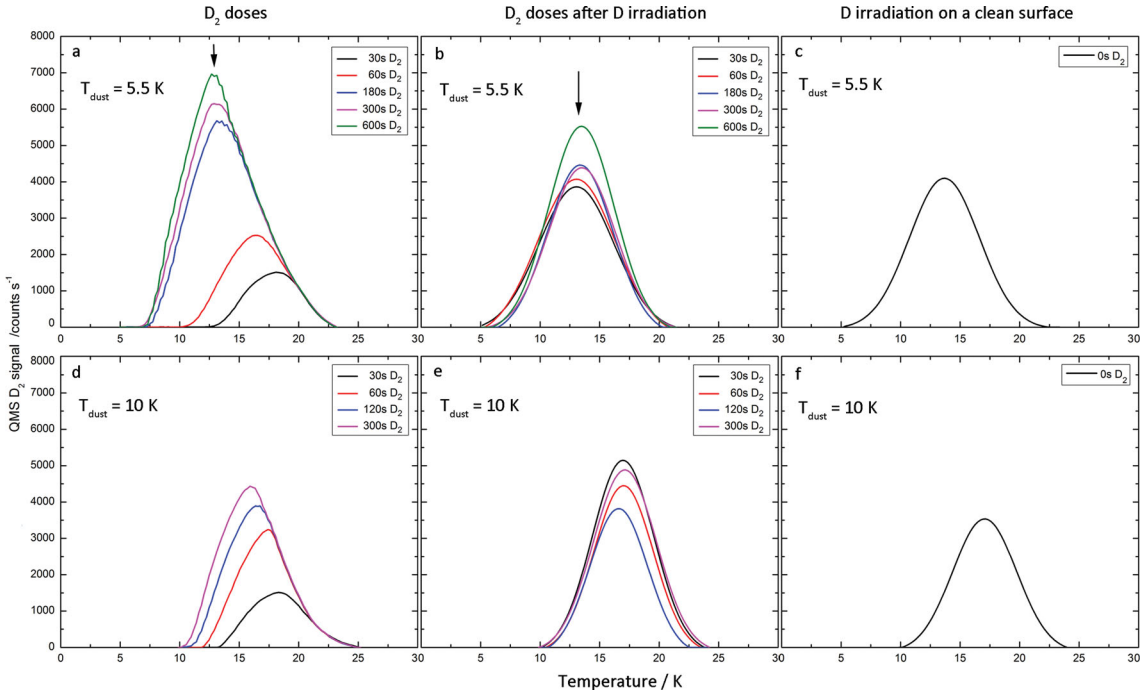

Figure 3. TPD profiles for D_2 (mass of 4 a.m.u.) obtained with the QMS on a silicate sample at $T_{\rm dust} = 5.5$ K (top) and $T_{\rm dust} = 10$ K (bottom). Left: after pure D_2 irradiation. Centre: after irradiation for 1200 s with D atoms on top of D_2. Right: after irradiation for 1200 s with D atoms on top of a clean surface. The initial molecular dose irradiation times are listed in each inset. Arrows show TPD peaks after D irradiation on D_2 doses converging at the lower energy edge of the pre-coverage TPDs (see Section 3.2).

At $T_{\rm dust} = 5.5$ K the TPD profile peaks shift towards lower adsorption energies as the molecular exposure is increased. Although this is characteristic of a second-order desorption, in this case it is due to other effects, since molecular desorption obeys first-order kinetics. As soon as the first molecules encounter the surface they preferentially adsorb on the enhanced binding sites either directly or after migrating on the surface. As the coverage is increased, lower binding energy sites get populated. We explain this phenomenon by considering that D_2 molecules arrive at the surface with certain thermal energy. Following the collision, the molecule either scatters back into the gas phase (elastically or inelastically) or is trapped in the region close to the surface. If the latter happens, Harris & Kasemo (1981) proposed that a particle performs a random walk on the surface during which energy is continuously exchanged between the various degrees of freedom of the system. On the other hand, the Langmuir–Hinshelwood mechanism shows that migration on surface can happen via thermal diffusion. The particle hops parallel to the surface to other sites until it arrives on a site deep enough where it cannot diffuse out from, effectively thermalizing. Both mechanisms explain why particles seem to preferentially land on deeper adsorption sites: it is the last step of diffusion on the surface. Alternatively, a shift in the TPD traces can also be produced by the interaction between molecules (Kolasinski 2008). At both surface temperatures the deuterium molecules are

unable to form a multilayer of D_2, given that the desorption rate is as high as 0.37 ML s^{-1} for the surface at 5.5 K (Schlichting & Menzel 1993).

Solutions of equation (5) give the peak desorption energy range for D_2 molecules. Assuming a desorption efficiency factor $A = 10^{12}\,s^{-1}$, given by the fundamental vibration frequency of a molecule on the surface, the desorption energies at the TPD peaks range from 32 to 46 meV, from larger to smaller dose at 5.5 K. At 10 K the corresponding desorption peak energies range from 39 to 46 meV. We also note a 1-K shift in the trailing (high-temperature) edge of the TPD profiles for doses at 10 K compared to doses at 5.5 K. A single measurement at 16 K confirms this shift, due to a higher thermal diffusion rate allowed by the hotter surface. Lemaire et al. (2010) showed that two mechanisms compete in the formation of molecules on dust at different surface temperatures. Recombination at higher surface temperature is likely due to the Harris–Kasemo mechanism, which allows the non-thermal diffusion of particles on the surface. At higher surface temperature, this diffusion will be further enhanced, as the atoms will take on the energy from some of the enhanced vibrational modes of the surface. This increases the length of the random walk and thus the possibility of being trapped in even more energetic binding sites. We think a similar mechanism is at play when molecules populate a surface at higher temperature.

3.2 Irradiation with deuterium atoms

Following irradiation with atoms on the pre-covered surfaces (Fig. 3, centre), the TPD peaks for D_2 converge around 32–33 meV for experiments at 5.5 K and around 41–42 meV for experiments at 10 K. We note a shift in the trailing TPD edge of about 3 K at a surface at 10 K, due to the combined effect of enhanced atomic and molecular diffusion compared to the surface at 5.5 K.

Following irradiation with atoms on a clean surface (Fig. 3, right-hand panel), the TPD peak is centred at 33 meV at 5.5 K and at 44 meV at 10 K. Thus, the resulting TPD profiles after 1200 s of atomic irradiation on the pre-dosed surfaces are more affected by the atomic irradiation for 1200 s than by the molecular population (doses $\leq$ 600 s).

Irradiation with atoms on a pre-dosed surface leads to TPD profiles peaking around the same desorption temperature (see arrow at 13 K in Fig. 3b). This temperature corresponds to the TPD peak of the largest molecular pre-coverage dose, e.g. the peak is at 13 K for irradiation of 600 s at 5.5 K too (Fig. 3a). This is because recombination-induced desorption preferentially targets the lower energy edge of the D_2 pre-adsorbed doses, as seen on Fig. 6. This effect is more prominent for larger pre-adsorbed D_2 doses, and it is optimized for the dose before saturation.

3.3 D_2 formation enhancement

We process the QMS signal (D_2 in all quantum states) and the REMPI signal (newly formed, excited D_2) during interval (b) (see Fig. 1) corresponding to the irradiation of the D_2 pre-covered surface with D atoms. In this interval recombination happens promptly and we detect an REMPI signal as soon as atomic exposure starts. Conversely, we did not detect REMPI signals above the background level during the heating activated phase (the TPD).

Fig. 4 shows the QMS signal (gas-phase D_2) during interval (b), at $T_{\rm sample} = 5.5$ and 10 K after different D_2 pre-coverage doses. The QMS signal during atomic irradiation is the net result of (i) $N_{\rm D_{2,beam}}$, the undissociated fraction of the deuterium beam that is reflected from the surface, (ii) $N_{\rm D_{2,dose}}$, the ejected D_2 pre-coverage dose and (iii) $N_{\rm D_2{}^*}$, the newly formed D_2 molecules desorbing from the surface either excited or after being thermalized on the surface.

For the clean surface (no D_2 pre-coverage), the adsorbed D_2 molecules due to the undissociated beam fraction increases the sticking coefficient of D atoms and causes them to recombine more efficiently (Govers et al. 1980; Amiaud et al. 2007). For the pre-covered surfaces at 5.5 K, the maximum prompt recombination enhancement occurs for the 180 s and higher D_2 doses, up to 40 $\pm$ 5 per cent after 50 s, obtained by comparing to the QMS signal during atomic irradiation on a clean surface. From Fig. 4 we also note that at 10 K the maximum enhancement is about 25 $\pm$ 5 per cent after 50 s.

Each QMS curve reaches a steady state that corresponds to the attainment of a steady detection in the gas phase due to a maximum recombination rate which will be balanced by the surface ejection

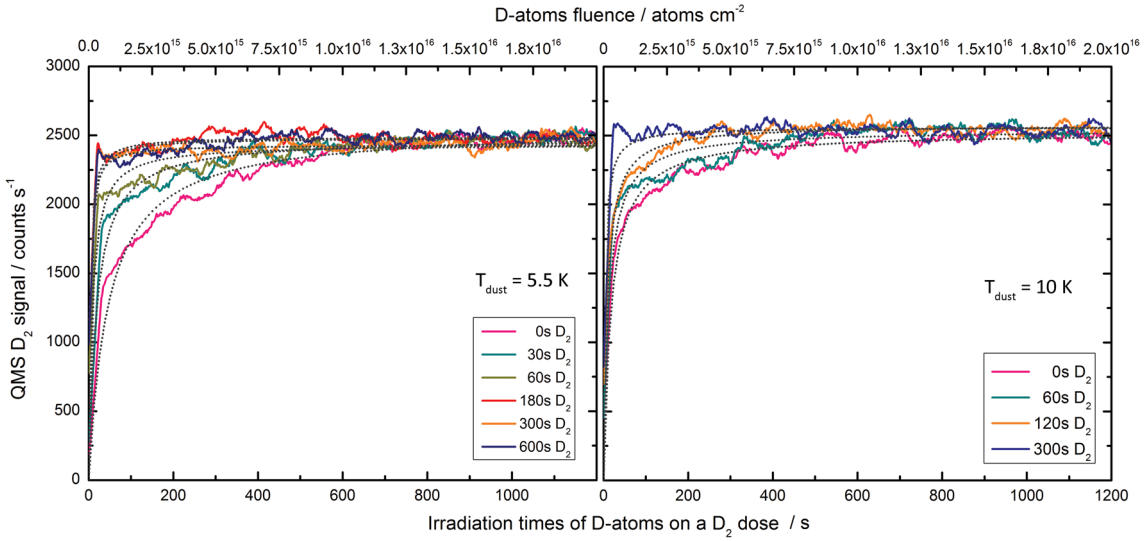

Figure 4. QMS signal of D_2 after a D_2 dose for x seconds (see inset) on the silicate surface, during irradiation with D atoms (Fig. 1, interval b) at 5.5 K (left) and 10 K (right). The 30-s curve at 10 K is omitted due to random detector noise, but the actual dose is verified by a TPD.

Table 1. Fitted parameters for hyperbolic fits of [QMS signal $(t) = P_1\, t/(P_2 + t)$] describing the QMS signal time evolution during irradiation with D atoms after D_2 doses.

D_2 on $T_{dust} = 5.5$ K (s)	P_1	P_2	D_2 on $T_{dust} = 10$ K (s)	P_1	P_2
0	2555	46.7	0	2525	18.3
30	2480	18.4			
60	2435	8.2	60	2540	12.2
180	2490	2.9	120	2575	8.7
300	2430	2.7	300	2560	3.1
600	2480	3.4			

of newly formed D_2 and the undissociated deuterium beam that elastically collides with the surface. The QMS signal time evolution curves are fitted by a hyperbolic function and the fitted parameters are given on Table 1. The fit to the rising QMS signal is given as

$$N_{D_2}(t) = \frac{P_1\, t}{P_2 + t}, \tag{6}$$

where P_1 is proportional to $N_{D_{2,beam}}$ and P_2 is proportional to $1/(N_{D_2*}, N_{D_{2,dose}})$. Since $N_{D_{2,dose}} \ll N_{D_2*}$, the inverse of the vertical asymptote parameter, P_2, is proportional to the recombination rate. The QMS curves have a higher steady-state level at $T_{dust} = 10$ K than at 5.5 K (2500 versus 2400 $\pm$ 50 count s^{-1} on average), and this can be explained by a shorter residence time causing an overall lower sticking coefficient.

For both surface temperatures we note that the QMS curves reach the steady-state level more rapidly for larger D_2 doses. This faster rise depends on the decreasing sticking coefficient of the exposed D_2 beam fraction on larger pre-adsorbed doses of D_2. It is also a function of the newly formed D_2 molecules and the recombination-induced desorbed pre-covered D_2 molecules. However, comparing Fig. 4, D_2 signals during D irradiation after D_2 doses, to Fig. 2, D_2 signals during D_2 irradiation on a clean surface, we note that the QMS signal rises faster when we irradiate with atoms. The QMS signal rise is then dominated by the newly formed D_2 and the ejected D_2 from the pre-coverage and less influenced by the decreasing sticking of undissociated D_2 from the beam. We use REMPI as a complementary detector since it is difficult to determine if the faster rise to the steady state is due to the newly formed D_2 from the QMS curves alone.

While the amount of particles detected due to D_2 recombination depends on the constant incoming D-atom flux, the amount of ejected pre-coverage depends on the molecular dose that was previously adsorbed (less than a D_2 monolayer for the maximum dose). Since recombination is an exothermic reaction, towards the end of irradiation with D atoms, the pre-coverage will be completely ejected (as it will be shown from the TPD analysis below), and the instantaneous coverage will be similar for all experiments. We indeed see a convergence of the QMS curves for all initial doses at a fluence $\sim 10^{16}$ atoms cm^{-2} or 700 s of D-atom irradiation at 5.5 K and after 500 s at 10 K (Fig. 4).

The time evolution of the REMPI signals show the abundance of newly formed D_2 molecules detected in the selectively ionized rovibrational level $v'' = 2$, $J'' = 4$. At $T_{dust} = 5.5$ K, there is a significant difference for curves that follow a dose of pre-adsorbed D_2 compared to the curve that corresponds to a clean surface (Fig. 5, left-hand panel). It occurs from the very start of atomic irradiation (at 50 s) and can be as large as 40 $\pm$ 10 per cent compared to the REMPI curve following no dose, and 30 $\pm$ 10 per cent at 10 K. However, after about 1000 s of irradiation with atoms at 5.5 K and after 500 s at 10 K, we see that there is a tendency for the curves to converge to the curve with no pre-dosing of D_2. This confirms the trend in the QMS signals, assuming that the atomic irradiation has cleaned up the entire surface from the initial doses via recombination-induced desorption.

The REMPI curves for all doses show a rapid increase to a maximum signal level at a fluence of $\sim 5 \times 10^{15}$ molecules cm^{-2} at 5.5 K, reaching steady state. The REMPI curves at $T_{dust} = 10$ K show a formation enhancement which begins to vanish rapidly at a fluence of $\sim 2 \times 10^{15}$ molecules cm^{-2}. We also note that the time to reach the steady state seems to be longer for the REMPI curves than for the QMS curves. This is due to the fact that the QMS rise is coupled to the decreasing sticking coefficient due to the presence of other (non-nascent) D_2 molecules. Thus, the REMPI-TOF detector allows us to confirm that formation is enhanced at higher molecular

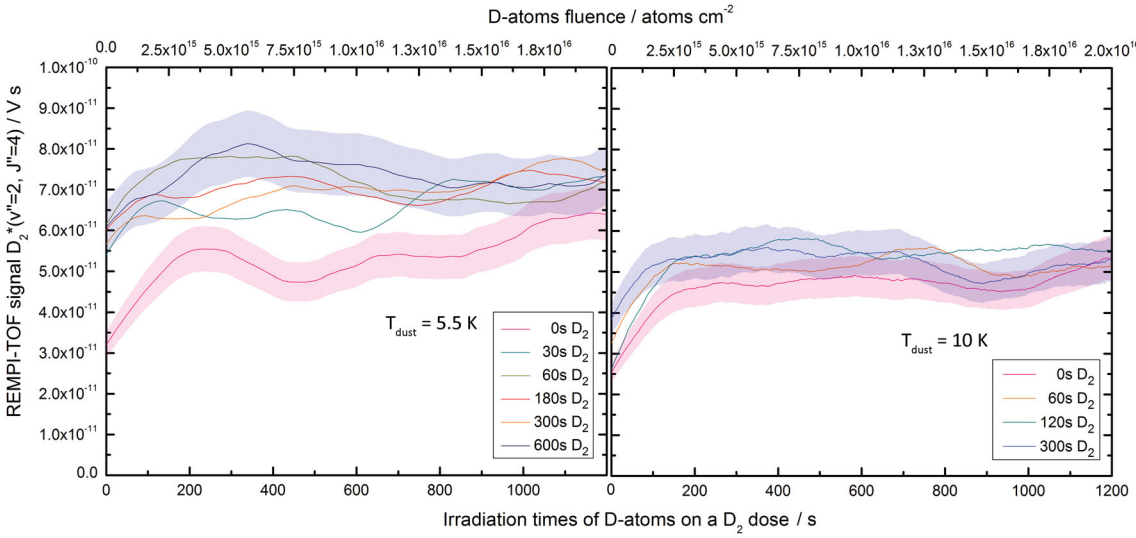

Figure 5. REMPI-TOF signal of excited D_2* due to recombination on the silicate surface as a function of irradiation of D atoms on top of a surface pre-dosed with D_2 (see inset for the doses used). At left, data are for a surface at $T = 5.5$ K; at right, for a surface at $T = 10$ K. The coloured bands are the respective error bars for the lowest and largest REMPI signals at each sample temperature. The lower bands are the error margins for D_2* on a clean surface.

pre-coverage. Furthermore, it allows us to disentangle the D_2 formation signal in two components: the prompt recombination-induced desorption and the undissociated fraction of the incident beam. This would not be possible with the QMS alone.

3.4 Comparison to previous works

We contrast these results with previous experiments on D_2 recombination on an icy surface (Congiu et al. 2009). Atoms were irradiated on ice multilayers which were either porous or non-porous. The recombination signal monitored by a QMS showed a rapid increase (transient phase) followed by a decrease to 1/5 of the original signal. This was interpreted as the thermalization of newly formed D_2 on the pores of the rough ice surface. Roser et al. (2003) and Hornekær et al. (2003) also found evidence that nascent HD is thermalized on porous water ice.

The non-porous amorphous solid water (np-ASW) surface has been compared to the silicate surface via temperature programmed desorption (TPD) experiments. These showed similar saturation coverages of CO, O_2, H_2O and D_2 on both silicate and np-ASW water ice surfaces held at 10 K using the same flux (Chaabouni et al. 2012). The experiments on D irradiation on ASW (Congiu et al. 2009) were done using a QMS for which the ionizing electron energy is set to 15.2 eV. This would allow the detection of molecules in a vibrationally excited state $v'' \geq 2$. However, unlike that work, here we do not observe a transient behaviour of the recombination signal for the D_2 covered silicate, but instead a rapid increase to a steady-state level. This could be a consequence of the dominance of the non-thermal desorption rate due to recombination exoergicity. This difference could also be due to the lower signal by the smaller populations of rovibrationally excited particles at $v'' \geq 2$, compared to the optimally selected rovibrational state detected via REMPI or due to deeper surface chemical and morphological differences that are undetected by the TPD.

4 ANALYSIS

4.1 Model of D_2 formation

The REMPI-TOF detector enables us to distinguish the enhanced formation signal (excited D_2 at $v'' = 4$, $J'' = 2$) on a molecule pre-covered silicate. We attribute this to the enhanced diffusion of incoming atoms. This confirms the high mobility of atoms at low temperatures (Hornekær et al. 2003). Hydrogen atoms that arrive at the silicate surface can diffuse either via thermal hopping or quantum mechanical tunnelling (Cazaux & Tielens 2004).

The TPD analysis of the D_2 pre-coverage doses deposited at 10 K shows that at this temperature D_2 molecules can populate adsorption sites up to a range of 27–57 meV depending on the dose. The first dose of 30 s of D_2 is distributed on physisorption sites, peaking at 46 meV and extending to 57 meV, leaving empty physisorption sites between 27 and 46 meV ($\Delta E_{\rm ads} \sim 19$ meV). The 60-s dose leaves unoccupied physisorption sites between 27 and 43 meV ($\Delta E_{\rm ads} \sim 16$ meV). D_2 molecules are adsorbed by first occupying the more energetic sites at lower coverage. The adsorption energies for D_2 are found using equation (5), where the TPD peak is used to calculate the desorption energy independent of the initial coverage. The lower and upper limits on the adsorption energies were estimated by fitting the TPD profiles with the direct inversion method (Amiaud 2006).

Thermal diffusion occurs via the Langmuir–Hinshelwood mechanism and is related to the depth of the physisorption well of the initial adatom. For H_2 molecules on an amorphous surface the diffusion energy can be ~60 per cent of the molecular binding energy and ~50 per cent for atoms (Perets et al. 2007). The available sites following the smallest molecular pre-coverage dose have $E_{\rm ads} < 46$ meV. The diffusion barrier for incoming molecules would then be $E_{\rm diff} < 28$ meV, following this dose. Following larger doses, the available sites are restricted to the lower energy sites for incoming molecules, and so the diffusion energies are lowered.

For D atoms, the thermal diffusion barrier (assuming $E_{\rm diff}$ (D_2 ~ 50 per cent of $E_{\rm ads}$ (D_2) is reduced as the pre-coverage dose increases. We estimate $E_{\rm diff} > 14$ meV for all doses (calculated from the smallest adsorption energy of D_2 from the largest dose TPD). $E_{\rm diff} < 23$ meV following the smallest molecular dose and <20 meV towards the largest dose. Vidali et al. (2009) showed that there is an extensive range of recombination yields for different silicates due to morphology. He, Frank & Vidali (2011) found lower and more sharply distributed desorption energies from a single crystal versus an amorphous film. Therefore, we expect a large range of diffusion energies. Perets et al. (2007) used rate equations to calculate the diffusion energies and obtained unique values on an amorphous silicate: $E_{\rm diff}$ (H) ~ 35 meV, $E_{\rm ads}$ (H) ~ 44 meV and $E_{\rm ads}$ (H_2) ~ 53 meV. These are higher than those estimated here. Perets et al. (2005) calculated between 41 and 55 meV for H atoms on ASW. Matar et al. (2008) derived a single diffusion activation barrier at 22 meV for D atoms on ASW, while Watanabe et al. (2010) derived 18 meV for H atoms on ASW, and up to 50 meV for deep sites, confirming our current results.

While for thermal diffusion the diffusion energy is related to the depth of the physisorption barrier, quantum tunnelling is a function of the difference between the binding energies of two physisorbed sites. Cazaux et al. (2011) show that the diffusion rate for an atom to go from one physisorbed site to another physisorbed site ($R_{\rm pp}$) can be written as

$$R_{\rm pp} = \nu_{\rm p} \exp\left(\frac{-E_{\rm pp}}{k_{\rm B} T}\right), \quad (7)$$

where $\nu_{\rm p}$ is the oscillation factor of the atoms in the physisorbed site, taken as $\nu_{\rm p} = 10^{12}\,{\rm s}^{-1}$. The diffusion rate by tunnelling increases as $\Delta E_{\rm pp}$, the barrier between two physisorption sites, is lowered. Diffusion by tunnelling increases due to the progressive occupation of shallower sites by larger pre-coverage doses.

At 10 K, the maximum barrier for molecular diffusion is lowered from $\Delta E_{\rm ads} \sim 19$ meV for the lowest dose to $\Delta E_{\rm ads} \sim 12$ meV for the highest dose. For atoms, the barrier is then lowered from $\Delta E_{\rm ads} \sim 9$ to 6 meV. At 5.5 K, the physisorption barrier for atoms is reduced from $\Delta E_{\rm ads} \sim 15$ to 7 meV. These enhancements (33 per cent at 10 K and 47 per cent at 5.5 K) correspond to those detected using REMPI (see Section 3.3). The molecular pre-coverage thus enhances tunnelling as the atoms can access a subset of lower physisorption wells (as the energy level matching between sites is enhanced) compared to the average population.

4.2 Molecular ejection: D_2 feedback

We analyse the recombination-induced desorption of the pre-adsorbed D_2 by comparing the TPD profiles after each D_2 dose and after atomic irradiation on each D_2 dose (Fig. 3, left-hand and centre panels). For this comparison it is necessary to consider the TPD profile due to the irradiation of D atoms on a clean surface for 1200 s (Fig. 3, right-hand panel). This TPD is due to both the newly formed D_2 and D_2 from the undissociated beam.

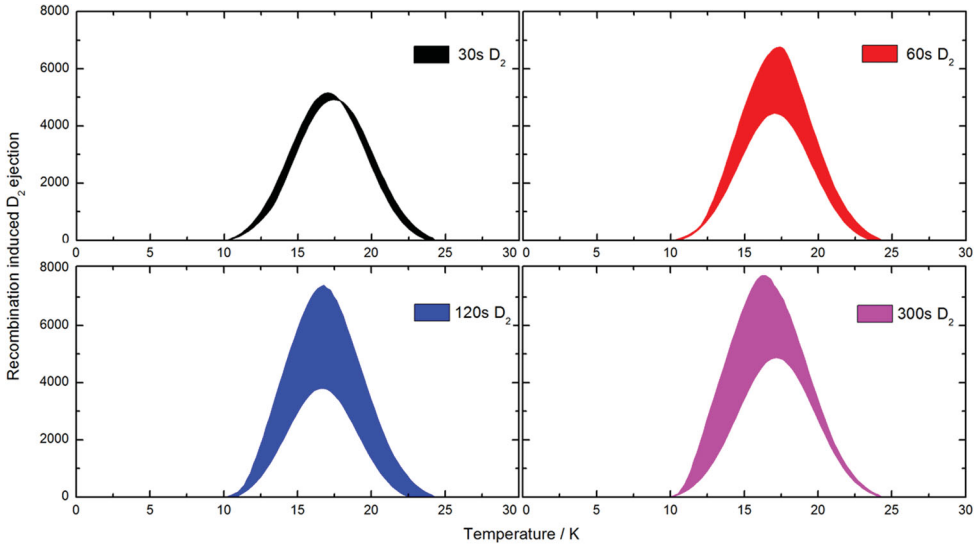

Figure 6. Net D_2 recombination-induced desorption at 10 K for each pre-coverage dose. The shaded areas correspond to the difference between the constructed TPD (see text) and the experimentally obtained TPD after irradiating D atoms for 1200 s on different D_2 doses. The areas show a preference for recombination-induced desorption on D_2 molecules adsorbed on the less energetic sites. The largest recombination-induced desorption corresponds to the 120-s D_2 dose.

Thus, in order to compare the recombination-induced desorption of any D_2 stuck on the surface we sum the TPD due to 1200 s of D_2 on a clean silicate to the TPD due solely to each molecular dose. The resulting TPD for each dose would be obtained if we assumed no reactivity (no exothermic desorptions) between the recombined D_2 and the pre-coverage doses, in which case both contributions may be stacked and desorbed as one large TPD. We compare these constructed TPDs to the experimentally obtained ones (Fig. 3, centre). These later TPDs are experimentally obtained by irradiating with D atoms for 1200 s on each pre-covered dose.

We find specific molecular doses that maximize recombination-induced desorption: 300s D_2 at 5.5 K and 120 s D_2 at 10 K (see Fig. 6). This is due to the competition between enhanced diffusion on the lower energy binding sites after pre-covering the surface with D_2 molecules and the lower residence time that results from lower binding energies. Thus, at specific doses, recombination is maximized over the decreasing sticking coefficient. We propose that at the maximum coverage (surface saturation), atoms will diffuse more easily, but a large fraction will leave the surface before encountering another atom. At this pre-coverage, the decreased sticking will dominate over recombination. Fig. 6 also shows that the net recombination-induced desorption is targeted to the less energetically bound populations, i.e. the 4.48 eV released in each recombination will desorb more molecules that are less energetically adsorbed, as expected.

We further calculate the desorption of all possible molecular D_2 that could be stuck on the surface from the beginning of the molecular dosing. This includes the initial molecular dose, the contribution of the undissociated beam and the nascent thermalized D_2 after 1200 s of irradiation with D atoms. We do this by comparing the total area (the number of absorbed molecules) under all TPD profiles (calculated and experimentally obtained). These results are shown in Fig. 7. We fit these trends with a polynomial, showing the specific D_2 pre-coverages that maximize desorption: 200 s or 1.5×10^{15} molecules cm^{-2} at $T_{dust} = 5.5$ K and 400 s or 3.2×10^{15} molecules cm^{-2} at $T_{dust} = 10$ K. These doses correspond to the dominance of the recombination-induced desorption over the

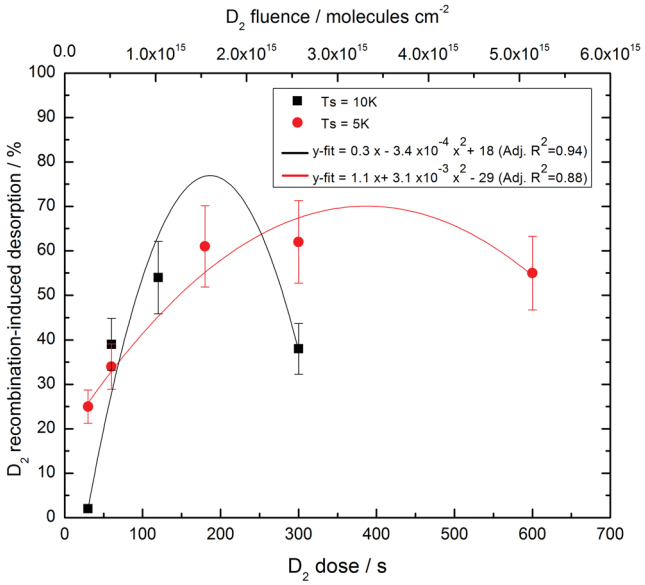

Figure 7. Per cent of the net molecular coverage on the surface (from the beginning of each experiment) ejected by D_2 recombination on the silicate dust surface at $T_{dust} = 5.5$ and 10 K after irradiation with D atoms for 1200 s. This molecular coverage (solid-phase D_2) includes the pre-coverage D_2 dose, the newly formed D_2* molecules that thermalize and D_2 from the undissociated beam that sticks on the surface.

thermalization rate. The desorption after $\sim 10^3$ s or an exposed D-fluence of 2×10^{16} atoms cm^{-2} ranges from 25 to 65 per cent of all D_2 sticking on the surface in this interval at 5.5 K and from 2 to 70 per cent at 10 K.

Garrod et al. (2007) estimated the branching fraction of desorption due to exothermic reactions by using the Rice–Ramsperger–Kessel (RKK) theory (Holbrook 1996). This theory for unimolecular gas reactions treats the surface-molecule bond as an additional molecular vibrational mode. Here, the probability of non-desorption (i.e. that there is a surface bond with energy greater than the

exothermic energy release) is given by

$$P = \left(1 - \frac{E_{\rm D}}{E_{\rm reac}}\right)^{s-1}, \quad (8)$$

where $E_{\rm D}$ is the desorption energy (binding energy to the silicate) of the product molecule (pre-adsorbed D_2 in our case), $E_{\rm reac}$ is the energy of formation released in the reaction and s is the number of vibrational modes in the molecule/surface-bond system. For diatomic species $s = 2$. The fraction of desorbed products is then given by

$$f = \frac{aP}{1 + aP}, \quad (9)$$

where a is a parameter usually taken as 1, and since $E_{\rm D}$ is usually less than $E_{\rm reac}$, $P \sim 1$ and $f \sim a$. Garrod et al. (2007) took $a =$ 0, 0.01, 0.03 and 0.1, or a maximum desorption fraction of 10 per cent per exothermic reaction. Our experiments show that an approximation like RKK for recombination-induced desorption does not account for effects like time-dependent surface coverage and the non-linearity of recombination enhancements. We note that we use a similar order of magnitude flux for atoms as for molecules. In the ISM, the gas-phase abundances of D atoms are much lower than the gas abundances of D_2 molecules (Kristensen et al. 2011), so our net recombination/desorption effect will have to be scaled down.

An upper limit of 1 eV into translation energy was obtained from the QMS temporal widths of the H_2 and HD signals on a HOPG surface (Creighan et al. 2006). Combining this upper limit on the translational energy with the internal energy of the maximum (v'', J'') populated levels observed in that experiment, it was suggested that an upper limit of approximately 40 per cent of the binding energy released upon the formation of H_2 (and HD) goes into internal (0.8 eV) and translational (1 eV) excitation of the detected molecules, with the remainder (2.7 eV) of the energy flowing into the HOPG surface. The energy partition of recombined D_2 on an amorphous silicate surface may differ, but these values can be compared as hydrogen isotopologues are electronically equivalent. However, it is possible that molecular hydrogen formed by diffusion on shallow wells will most likely desorb with large internal energy, while molecular hydrogen formed on deeper wells may thermalize and impart most of its energy to the grain.

5 ASTROPHYSICAL IMPLICATIONS

Our experiments elucidate the parameters involved in the accelerated recombination of deuterium and the ensuing ejection of D_2 molecules from a pre-adsorbed molecular dose. This scenario is common in low-temperature ISM environments where dust will develop icy mantles as molecules condense on its surface. The enhanced gas feedback mechanism due to recombination-induced desorption is proposed as an important surface reaction leading to the increasing abundance of D_2 in these regions.

Deuterium chemistry plays a pivotal role in cold ISM environments like dense molecular core nuclei. Deuterium fractionation in dense cores is the isotopic enhancement of deuterium over hydrogen, seen in about 25 deuterated molecules (Millar 2003). Although the deuterium reservoir is provided by HD, towards denser regions, D_2 can become a significant deuterium reservoir (Roueff et al. 2005). In hot cores, deuterium fractionation has been proposed as a result of the evaporation of deuterium-rich molecules from icy grain mantles by the new star. However, recombination-induced desorption can be a non-trivial evaporation mechanism of D_2 during the pre-stellar core (PSC) phase, consequently reducing the gas abundance in the protostellar, activated heating, phase. PSCs are typically cold ($\leq$10 K) and have number densities $\geq 10^4$ H_2 molecules cm^{-3} (e.g. Ward-Thompson et al. 1994; Crapsi et al. 2005). It was previously thought that low temperatures in PSCs do not allow significant evaporation to occur. It has been shown that in these regions recombination-induced desorption can dominate over non-thermal desorption processes such as cosmic rays and photodesorption (Garrod et al. 2007).

The abundance of molecular hydrogen and isotopologues on dust grains in the dense ISM regions has been recently estimated (Kristensen et al. 2011). This work is based on experiments on a porous ASW ice surface (10 ML) at 10 K (comparable to a processed thicker mantle in the ISM). Since their model assumes thermodynamical equilibrium at each step (a stationary approach), and allows only one molecule per adsorption site, the population is given in the Fermi–Dirac formalism. At $n(H_2) = 10^6$ cm^{-3}, the average abundance in a PSC deuteration zone, they estimate the ratio of D_2 to H_2 on the surface to be $\sim$30 times greater than in the gas phase, implying an atomic fractionation 60 times larger than in the gas phase. The ratio of HD/H_2 remains almost constant both in the solid and gas phase. This amounts to a greater D/H abundance in the solid phase due to the higher zero-point energy of D_2 (2.6 meV greater than HD), making it more strongly bounded. Since the deuterium solid–gas phase ratio is greater than other isotopologues, the molecular coverage effect on recombination and recombination-induced desorption will be more targeted to D atoms than other hydrogen isotopes. This allows deuterium atoms to preferentially recombine and mine the solid D_2 reservoir on the ice mantles over other isotopes.

Our experimental results on enhanced formation also imply an accelerated depletion of the atomic hydrogen reservoir towards denser ISM regions. We could reinterpret the results obtained on deuterium recombination on np-ASW (Congiu et al. 2009) where it is argued that the thermalization of newly formed D_2 molecules explains the non-detection of D_2 in dark clouds. Instead, we argue that the formation enhancement caused by the pre-adsorbed or frozen D_2 molecules on dust will deplete the atomic reservoir, and if the density of atoms is reduced, recombination will not be detectable. This supports the theory put forward by Islam et al. (2010). In this work, a chemical model is used to predict environments where a signature of the H_2 formation process can be detected. Dark clouds are not suitable since the atomic reservoir is too low for viable rovibrationally excited H_2 detection via IR fluorescence. Instead, environments which contain X-ray sources, with adequate electron densities to dissociate hydrogen molecules, would supply sufficient H atoms that can then recombine. The coupled effect of an enhanced formation rate and pre-adsorbed molecular ejection will result in larger molecular gas-phase abundances and a depleted atomic reservoir. This has important consequences in deuterium fractionation and the eventual retardation of molecular freeze-out on dust grains, an important condition in pre-protostellar core collapse (Flower, Pineau Des Forêts & Walmsley 2005).

6 CONCLUSIONS

Previous theoretical work examining molecular hydrogen formation on pristine dust surfaces has assumed that a molecule-saturated surface halts recombination due to short atomic residence times. We find instead a positive correlation between D_2 sub-monolayer doses on an amorphous silicate surface and D_2 formation, which can be up to 35 $\pm$ 10 per cent at $T_{\rm dust} = 5.5$ K. Furthermore, the non-thermal desorption due to D_2 recombination can lead to gas-phase feedback of up to a D_2 monolayer (approximately 10^{15} molecules cm^{-2}).

We employ an REMPI (2+1) quantum selective detector and a QMS detector during irradiation with atoms. The prompt recombination enhancement is confirmed by both instruments up to 1000 s of irradiation with atoms. We interpret this as the time when all molecular pre-coverage doses are completely ejected by the D_2 recombination-induced desorption. A complete TPD analysis provides the coverage profile before and after irradiation with D atoms on the D_2 dosed surface showing that recombination-induced desorption is enhanced by molecular doses below surface saturation. Finally, we show that molecule-covered dust grains remain active catalysts, enhancing recombination which desorbs condensates efficiently. The cycle of D_2 ejection due to enhanced D_2 recombination on cold silicates is a highly energetic process that can affect the chemical balance of the ISM prior to star formation.

ACKNOWLEDGMENTS

We thank Lionel Amiaud for his helpful insights into the estimation of the adsorption energies. The authors acknowledge the financial support from the Agence Nationale de la Recherche (ANR, contract 07-BLAN-0129), the Conseil Régional d'Île de France (SESAME contract I-07-597R), the Conseil Général du Val d'Oise and the French National PCMI program funded by the CNRS. GV acknowledges partial support by NSF Astronomy & Astrophysics Division, grant no. 0908108. LG is supported by the European Community FP7-ITN Marie-Curie Programme (LASSIE project, grant agreement no. 238258).

REFERENCES

Accolla M. et al., 2011, Phys. Chemistry Chemical Phys., 13, 8037
Amiaud L., 2006, PhD thesis, Univ. Cergy-Pontoise and Observatoire de Paris
Amiaud L., Dulieu F., Fillion J.-H., Momeni A., Lemaire J. L., 2007, J. Chemical Phys., 127, 144709
Brown W. L. et al., 1982, Nuclear Instrum. Methods Phys. Res., 198, 1
Cazaux S., Spaans M., 2004, ApJ, 611, 40
Cazaux S., Tielens A. G. G. M., 2004, ApJ, 604, 222
Cazaux S., Morisset S., Spaans M., Allouche A., 2011, A&A, 535, A27
Chaabouni H., Bergeron H., Baouche S., Dulieu F., Matar E., Congiu E., Gavilan L., Lemaire J. L., 2012, A&A, 538, A128
Congiu E., Matar E., Kristensen L. E., Dulieu F., Lemaire J. L., 2009, MNRAS, 397, L96
Crapsi A., Caselli P., Walmsley C. M., Myers P. C., Tafalla M., Lee C. W., Bourke T. L., 2005, ApJ, 619, 379
Creighan S. C., Perry J. S. A., Price S. D., 2006, J. Chemical Phys., 124, 114701
Dalgarno A., 1999, in Combes F., Pineau des Forêts G., eds, H2 in Space. Cambridge Univ. Press, Cambridge
Demtröder W., 1991, Laser Spectroscopy. Springer-Verlag, Berlin
Djouadi Z., D'Hendecourt L., Leroux H., Jones A. P., Borg J., Deboffle D., Chauvin N., 2005, A&A, 440, 179
Duley W. W., Williams D. A., 1993, MNRAS, 260, 37
Fantz U., Wunderlich D., 2004, Laser Spectroscopy. IAEA
Flower D. R., Pineau Des Forêts G., Walmsley C. M., 2005, A&A, 436, 933
Garrod R. T., Wakelam V., Herbst E., 2007, A&A, 467, 1103
Gould R. J., Salpeter E. E., 1963, ApJ, 138, 393
Goumans T. P. M., Bromley S. T., 2011, MNRAS, 414, 1285
Govers T. R., Mattera L., Scoles G., 1980, J. Chemical Phys., 72, 5446
Harris J., Kasemo B., 1981, Surface Sci., 105, L281
Hasegawa T. I., Herbst E., 1993, MNRAS, 261, 83
He J., Frank P., Vidali G., 2011, Phys. Chemistry Chemical Phys., 13, 15803
Holbrook K. A., 1996, Unimolecular Reactions, 2nd edn. Wiley, New York
Hollenbach D., Salpeter E. E., 1971, ApJ, 163, 155
Hornekær L., Baurichter A., Petrunin V. V., Field D., Luntz A. C., 2003, Sci, 302, 1943
Islam F., Latimer E. R., Price S. D., 2007, J. Chemical Phys., 127, 064701
Islam F., Cecchi-Pestellini C., Viti S., Casu S., 2010, ApJ, 725, 1111
Katz N., Furman I., Biham O., Pirronello V., Vidali G., 1999, ApJ, 522, 305
Kolasinski K. W., 2008, Surface Science: Foundation of Catalysis and Nanoscience. Wiley, New York
Kreckel H., Bruhns H., Čížek M., Glover S. C. O., Miller K. A., Urbain X., Savin D. W., 2010, Sci, 329, 69
Kristensen L. E., Amiaud L., Fillion J.-H., Dulieu F., Lemaire J.-L., 2011, A&A, 527, A44
Langmuir I., 1918, J. Am. Chemical Soc., 40, 1361
Latimer E. R., Islam F., Price S. D., 2008, Chemical Phys. Lett., 455, 174
Lee T. J., 1972, Nat, 237, 99
Lemaire J. L., Vidali G., Baouche S., Chehrouri M., Chaabouni H., Mokrane H., 2010, ApJ, 725, L156
Malmasson D., 1994, PhD thesis, Univ. Paris XI and Observatoire de Paris
Matar E., Congiu E., Dulieu F., Momeni A., Lemaire J. L., 2008, A&A, 492, L17
Millar T. J., 2003, Space Sci. Rev., 106, 73
Norman C. A., Spaans M., 1997, ApJ, 480, 145
Öberg K. I., Fuchs G. W., Awad Z., Fraser H. J., Schlemmer S., van Dishoeck E. F., Linnartz H., 2007, ApJ, 662, L23
Perets H. B., Biham O., Manicó G., Pirronello V., Roser J., Swords S., Vidali G., 2005, ApJ, 627, 850
Perets H. B. et al., 2007, ApJ, 661, L163
Perry J. S. A., Price S. D., 2003, Ap&SS, 285, 769
Pirronello V., Liu C., Shen L., Vidali G., 1997a, ApJ, 475, L69
Pirronello V., Biham O., Liu C., Shen L., Vidali G., 1997b, ApJ, 483, L131
Pirronello V., Liu C., Roser J. E., Vidali G., 1999, A&A, 344, 681
Pozgainer G., Windholz L., Winkler A., 1994, Measurement Sci. Technol., 5, 947
Roser J. E., Swords S., Vidali G., Manicò G., Pirronello V., 2003, ApJ, 596, L55
Roueff E., Lis D. C., van der Tak F. F. S., Gerin M., Goldsmith P. F., 2005, A&A, 438, 585
Schermann C., Pichou F., Landau M., Cadez I., Hall R. I., 1994, J. Chemical Phys., 101, 8152
Schlichting H., Menzel D., 1993, Rev. Sci. Instrum., 64, 2013
Vidali G. et al., 2007, J. Phys. Chemistry A, 111, 12611
Vidali G., Li L., Roser J. E., Badman R., 2009, Advances Space Res., 43, 1291
Ward-Thompson D., Scott P. F., Hills R. E., Andre P., 1994, MNRAS, 268, 276
Watanabe N., Kimura Y., Kouchi A., Chigai T., Hama T., Pirronello V., 2010, ApJ, 714, L233
Willacy K., Millar T. J., 1998, MNRAS, 298, 562

This paper has been typeset from a TEX/LATEX file prepared by the author.